A linear wheel–crossing interaction model

Citation for the original published paper (version of record):
Pålsson, B. (2018). A linear wheel–crossing interaction model. Proceedings of the Institution of Mechanical Engineers, Part F: Journal of Rail and Rapid Transit, 232(10): 2431-2443. http://dx.doi.org/10.1177/0954409718772984

A linear wheel–crossing interaction model

Björn A. Pålsson

CHARMEC/Division of Dynamics, Chalmers University of Technology, SE-412 96 Gothenburg, Sweden

Abstract

This paper presents the derivation of a linear model for wheel-rail interaction kinematics at railway crossings. The purpose of this model is to demonstrate the fundamental constraints imposed on crossing geometry if it should be compatible with a given range of wheel profile shapes. In this model the contact point locations on wing rail and crossing nose are described using linear functions and the wheel profiles are modelled as conical. Based on these assumptions, a method is developed to adjust the vertical position and longitudinal inclination of wing rail and crossing nose in order for the crossing geometry to be compatible with a given range of equivalent wheel profile cone angles. In particular, an expression is derived for the average impact angle. The derived relation highlights the potential of tailoring crossing geometries for a given spread in wheel profile shapes in traffic for minimized loading and damage. Further, the properties of the model are compared to results from quasi-static multi body simulations for a range of wheel profiles.

1. Introduction

Switches & Crossings (S&C) are vital components in railway networks as they provide flexibility to traffic operation by allowing trains to switch between tracks. The flexibility comes at a cost however as switch actuation and customized rail and bearer solutions increase complexity and cost. In addition, the wheel-rail transitions in S&C – from stock rail to switch rail and wing rail to crossing nose – cause higher wheel-rail contact forces and therefore higher rail degradation rates compared to regular track.

At crossings the increased loading is dominated by vertical impact loads which are related to a kink in the vertical wheel position trajectory. This kink is the result of the abrupt change in vertical travel direction that the wheel experiences when it makes the transition from wing rail to crossing nose (or vice versa). It is therefore of interest to shape the crossing geometry such that this kink is minimized as described in e.g.[1-3]. As demonstrated in[4] however, it is not possible to get rid of this kink and associated impacts if the crossing geometry is to be compatible with a range of wheel profile shapes.

The purpose of this paper is to further investigate the relation between requirements on the vertical positions and longitudinal inclinations of wing rail and crossing nose and the range of passing wheel profile shapes by employing a linear wheel-crossing interaction model. In particular, an expression is derived for the average impact angle that this range of wheel profiles will experience at the transition from wing rail to crossing nose in a crossing with a specified transition zone length and crossing angle.

2. The crossing problem

A fixed railway crossing constitutes a kinematic challenge in terms of the wheel–rail contact. The fact that two different rail and wheel paths intersect at one point requires that there exist flangeways which allow for the wheel flanges to pass through the crossing. Therefore the rails are split into a crossing nose and two wing rails. The overall layout of a crossing panel with the crossing in the middle is presented in Figure

1 together with a photograph of an in situ crossing. A top-view of a typical crossing layout as defined by its gauge corner contour is presented in Figure 2.

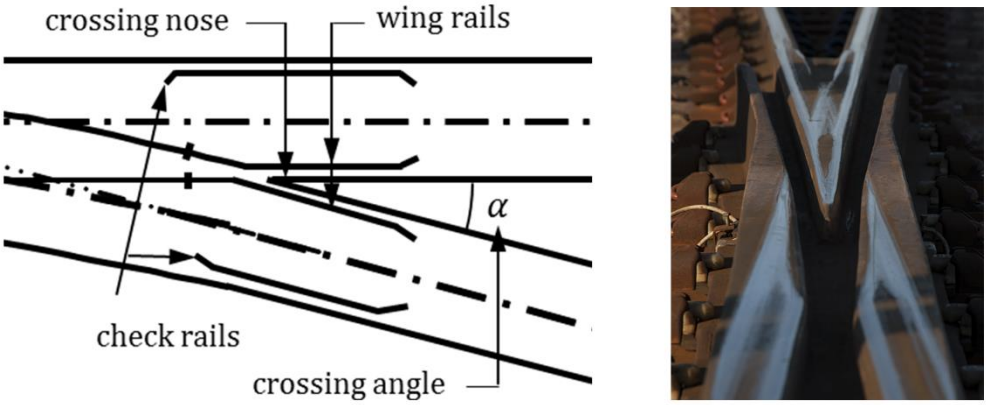

Figure 1. Sketch of a crossing panel (left), photo of a crossing in track (right)

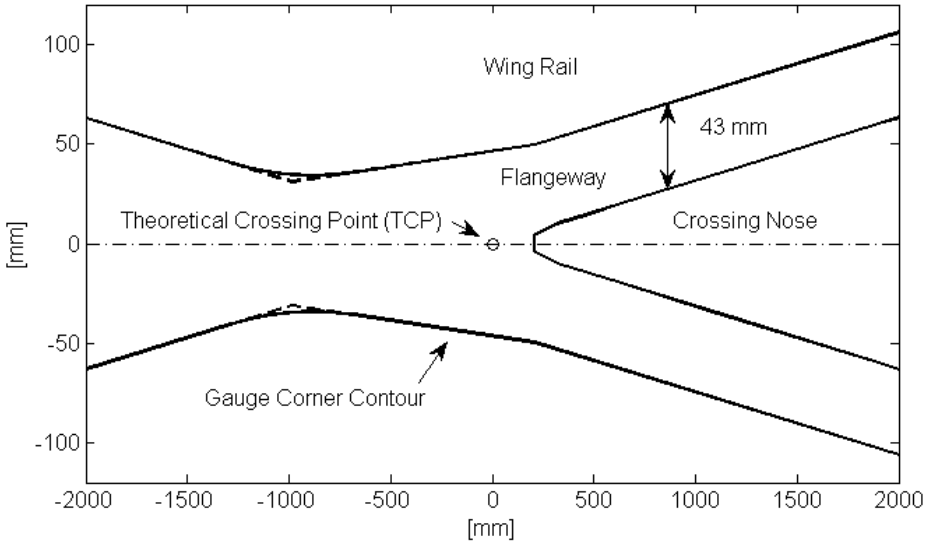

Figure 2. Top view of gauge corner contour at crossing

When a wheel passes over the crossing in the facing move (from the switch panel towards the crossing panel) it will first encounter the wing rail. Due to the outwards deviation of the wing rail, the wheel–rail contact point will move towards the outside of the wheel profile. For a typical conical wheel profile, the rolling radius will decrease and the wheel will move downwards. The reduced rolling radius on the crossing side will induce a yawing motion of the wheelset towards the crossing. Due to the check rail, the lateral motion of the wheelset is restrained and wheel flange interference contact with the crossing nose is prevented.

When the wheel reaches and makes contact with the crossing nose, the contact load is quickly transferred from the wing rail to the crossing nose. For a typical conical wheel profile, the rolling radius increases as the new contact point is close to the flange root. The two-point contact situation during the transition with contacts at different rolling radii induces relative tangential motion in the contacts that cause wear. The transition typically also results in a significant impact force on the crossing nose (or the wing rail depending on the traffic direction) as the slight downward motion of the vertical wheel

trajectory is reversed and the wheel is accelerated upwards by the crossing nose. Using eight cross-sections along a crossing, a schematic illustration of the crossing transition for a single wheel profile is illustrated in Figure 3. The vertical wheel positions at the different sections that form the vertical wheel trajectory are shown in Figure 4. The figure also illustrates the impact angle β.

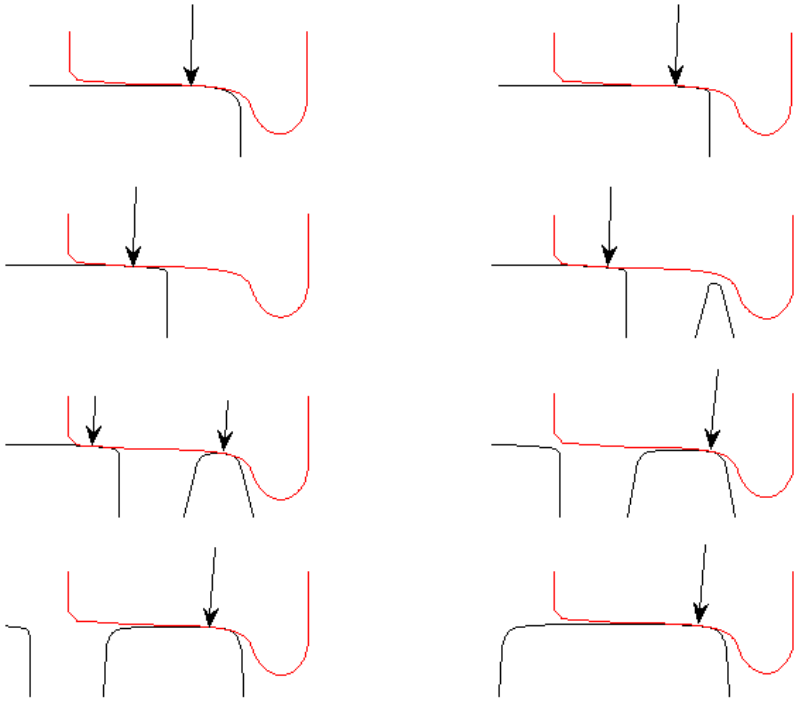

Figure 3. Schematic contact conditions and normal wheel–rail contact forces during a crossing transition

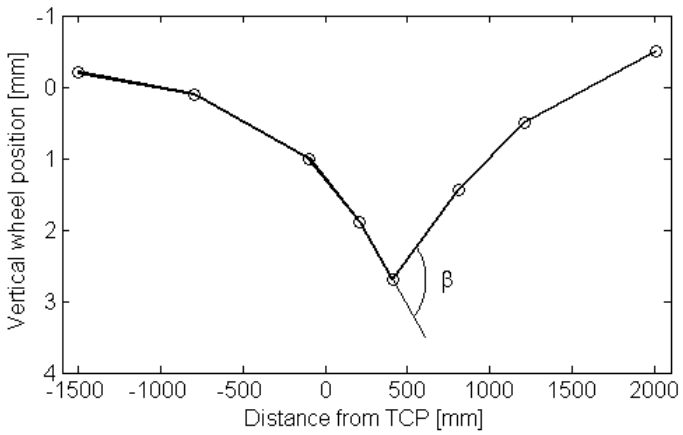

Figure 4. Vertical wheel trajectory corresponding to the vertical wheel positions of the cross-sections of Figure 3 as a function of distance from the Theoretical Crossing Point (TCP)

3. Wheel-crossing kinematics for a range of wheel profiles

The wheel-crossing interaction will naturally vary for different crossing and wheel profile geometries. In this section kinematic wheel-crossing interaction results are presented for 400 wheel profiles travelling over a generic crossing in order to illustrate this variation.

3.1. *Simulation model*

The wheel-crossing interaction kinematics have been evaluated in Multi Body Simulation (MBS) code Simpack[5]. The simulation model consists of a single rigid wheelset running in the through route of an S&C in the facing move (i.e. travelling straight and in the direction from wing rail to crossing nose). The wheelset is constrained laterally and in yaw and runs with a prescribed low velocity (0.1 m/s) in order to obtain quasi-static results.

The crossing geometry is a generic crossing geometry presented in[4] with a nominal crossing angle of 1/15 (corresponding to a turnout radius of 760 m). The overall layout of this crossing is taken from drawing 1-514 177 of the Swedish Railway Administration (Trafikverket) while the rail cross-sections have been optimized for minimum contact pressures.

The wheel profile set consists of 279 measured profiles from Regina passenger coaches[6], 120 measured profiles from freight wagons with Y25 bogies[7] and a nominal S1002 profile for a total of 400 profiles.

In traffic, wheelsets will typically exhibit a little yaw and lateral displacement which will affect the kinematics of the wheel-crossing interaction. Previously presented results[4] using the same crossing geometry and part of the wheel profiles utilized in this paper indicate that the longitudinal position of the transition point from wing rail to crossing nose can be shifted up to 15 mm for every millimetre of lateral wheelset displacement towards the crossing nose. The checkrail typically limits the lateral wheelset displacement to 3 millimetres in this direction. Larger lateral displacements are possible when the wheelset moves away from the crossing (as there is no constraint but the flange guidance towards this side), but the transition point is also less affected by lateral displacements in this direction[4].

It is thus a simplification not to consider the lateral wheelset displacement. However, as the objective of this paper is more oriented towards the nominal design of crossings and its fundamental constraints this is deemed to be a justifiable neglection to reduce complexity. A numerical study for a large population of measured wheel profiles that also incorporate the lateral displacement can be found here[8].

3.2. *Results*

Figure 5 illustrates the contact point trajectories for the 400 wheel profiles in the crossing transition area superimposed on a top view of the crossing's gauge corner contour. The trajectories of a nominal S1002 wheel profile and the most hollow worn wheel profile in the sample are highlighted. It can be observed that even though there is some spread in the lateral contact point locations on wing rail and crossing nose, the contact point bands are concentrated due to the design of the crossing geometry. The corresponding vertical wheel trajectories are presented in Figure 6. It can be observed that the vertical wheel trajectories are slightly parabolic on the wing rail and close to linear on the crossing nose.

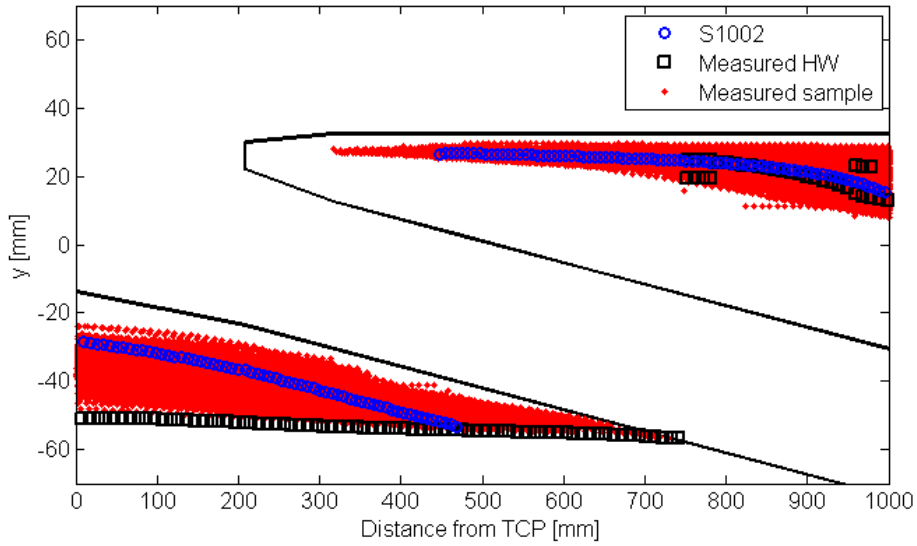

Figure 5. Top view of a crossing gauge corner contour horizontally oriented in the running direction with superimposed contact point trajectories for 400 wheel profiles. The upper part correspond to the crossing nose and the lower to the wing rail.

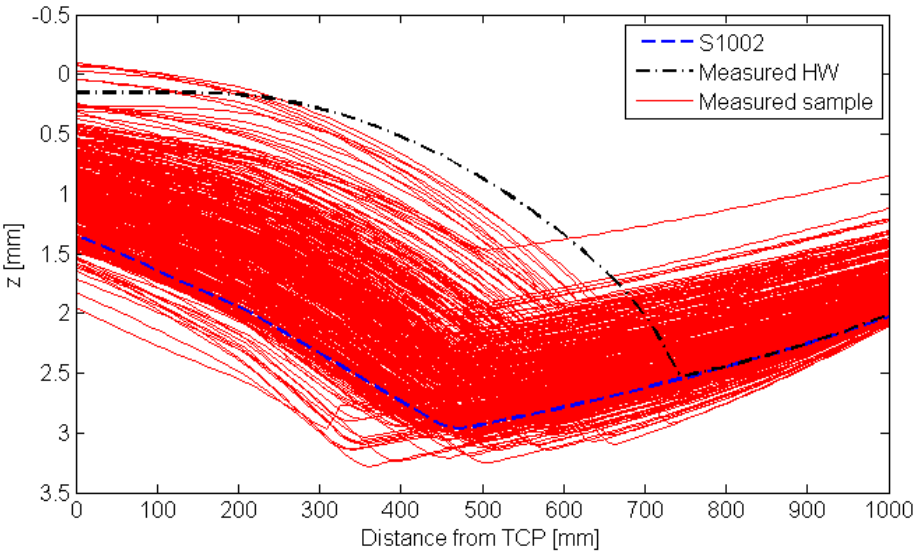

Figure 6. Vertical wheel trajectories as a function of the distance from the theoretical crossing point. Results for 400 wheel profiles

The difference in transition point between the nominal S1002 profile and the hollow worn profile can be explained by the height difference between the flange root and field side of these wheel profiles which correspond to the lateral contact point locations on wing rail and crossing nose. This difference is illustrated in Figure 7 together with equivalent cones fitted to each profile using representative lateral contact positions of $y_{\mathrm{cr}} = 25$ mm and y_{wr}=-55 mm on crossing and wing rail, respectively. These reference points are the same as previously used in[4]. The equivalent wheel profile cone angle φ is defined as

$$\varphi = \frac{z(y_{\mathrm{cr}}) - z(y_{\mathrm{wr}})}{y_{\mathrm{cr}} - y_{\mathrm{wr}}} \qquad (y_{\mathrm{cr}} = 25 \;\&\; y_{\mathrm{wr}} = -55) \qquad (1)$$

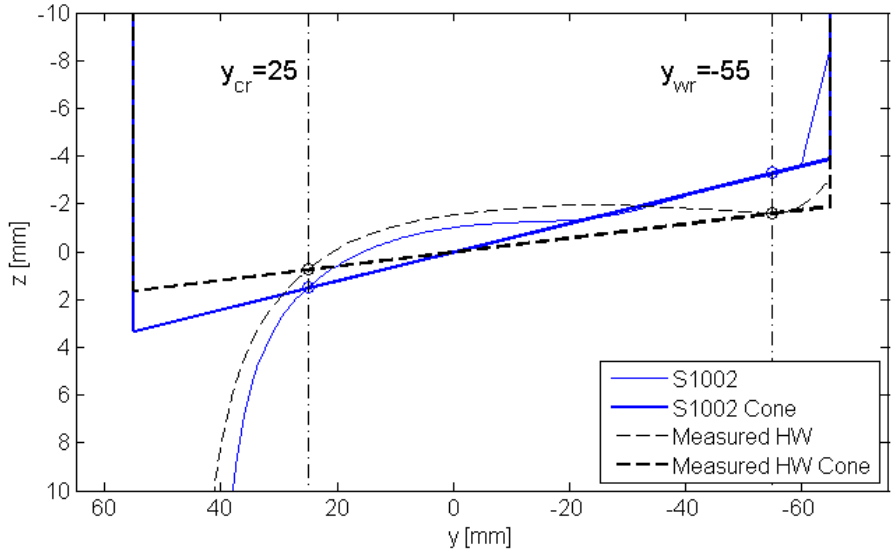

Figure 7. Detail of S1002 and hollow worn wheel profiles including fitted equivalent conical profiles

The upper graph of Figure 8 demonstrates the correlation between transition point and equivalent cone angle for the full wheel profile set. It can be observed that there is a strong correlation between these two parameters which is also demonstrated via the linear model fitted to the data points using the least squares method. The equation found via this regression is (with three value digits)

$$\varphi = -\frac{x}{9920} + 0.107 \qquad (2)$$

The lower graph in Figure 8 illustrates the distribution of transition points.

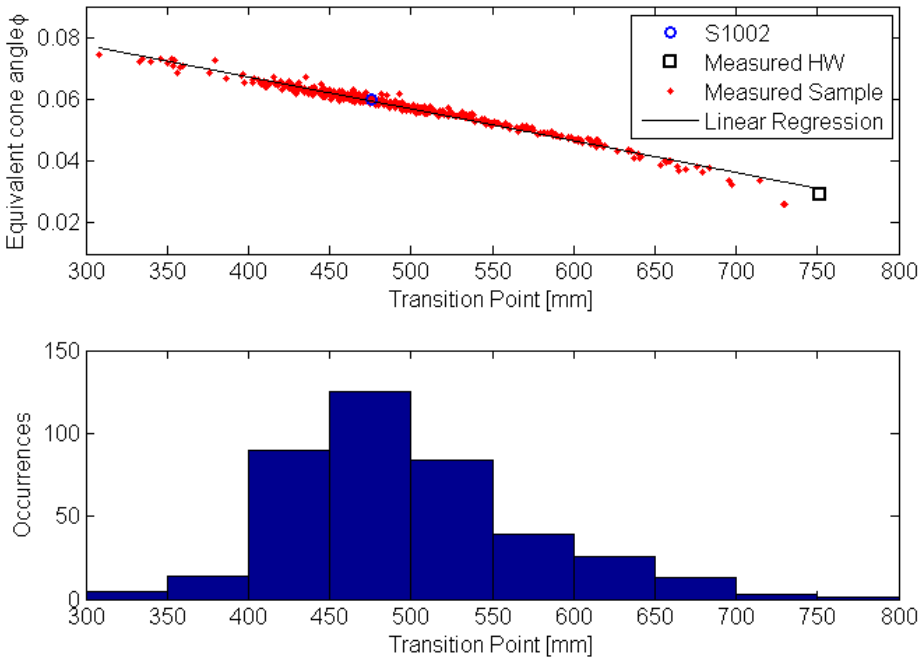

Figure 8. Wheel profile equivalent cone angle as a function of transition point (top). Histogram over transition point locations (bottom). Results for 400 wheel profiles

To summarise, the main results presented in this section are that

- The equivalent cone angle for a wheel profile correlate strongly with the profile's transition point.
- The contact bands on wing rail and crossing nose are concentrated due to the design of the crossing geometry.
- The vertical wheel trajectories on wing rail and crossing nose are close to linear around the transition points.

4. A linear model of wheel-rail interaction at crossings

Inspired by the observations in Section 3, a linear model will here be derived to allow for qualitative as well as quantitative study of wheel-crossing interaction and its fundamental geometric constraints. The model is based on the following simplifications of the wheel-crossing interaction.

- The wing rail and crossing nose are modelled as straight lines that only allow for one pre-defined contact point location per rail and longitudinal position.
- The wheel profiles are modelled as conical with an equivalent cone angle determined according to Eq. (1).
- A zero lateral wheel(set) displacement.

This modelling procedure allows for the derivation of analytical expressions for transition point and impact angle when a wheel passes over a crossing. It also allows for the derivation of a relation between the average impact angle $\bar{\beta}$ and a given range of wheel profile cone angles that should make an orderly crossing transition within a given transition zone. Previous analytical work to determine such relations have been presented by the present author in[4]. That work was based on geometrical reasoning and the work presented here can be seen as a mathematically more rigorous and general continuation of these efforts.

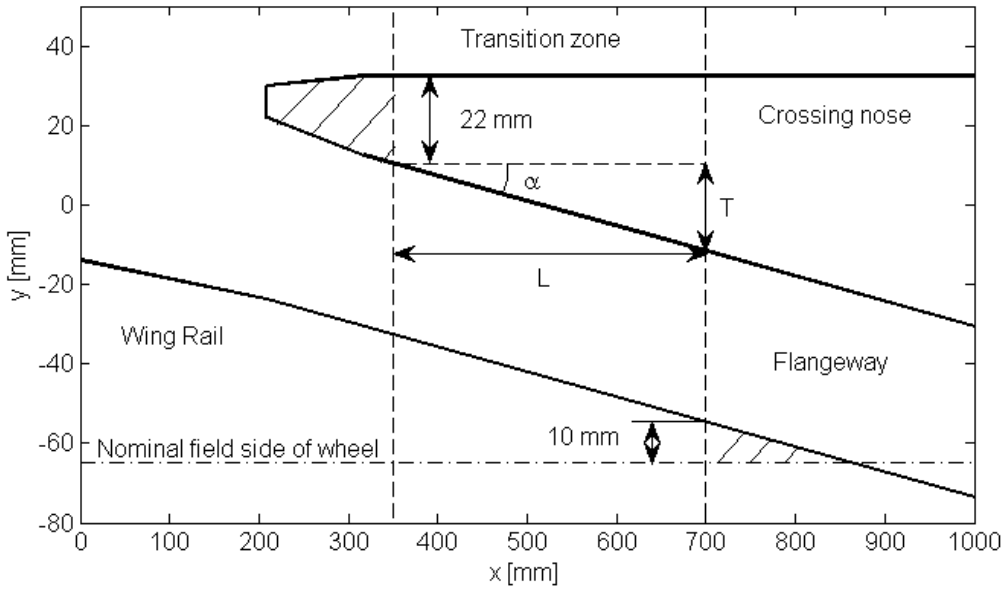

Figure 9. Top view of crossing geometry with crossing angle 1:15. TCP = Theoretical Crossing Point.

Figure 9 shows a schematic top view of a fixed crossing oriented along one of the traffic directions. The vertical dashed lines indicate the beginning and end of a nominal transition zone where it is preferred that passing wheels make their transition from wing rail to crossing nose and vice versa. The length of the transition zone is denoted L and the change in crossing nose width in the transition zone is denoted T. It can be observed

that T is an implicit measure of the transition zone length independent of α as L can be determined from a given T and α using the approximate tangent relation $\alpha \approx T/L$. T is also related to the change in overlap between a straight running wheel and the wing rail as the flange way has a constant width. The exact extension of the transition zone can vary, but it can be concluded that wheels should preferably not make contact with the crossing nose where it is too thin to carry the wheel load, and they should not make contact with the wing rail where the overlap between wheel and wing rail is too small to provide satisfying contact conditions. In this paper it is assumed that the feasible transition zone extends from where the crossing nose is 22 mm thick to where the overlap between wheel and wing rail is 10 mm. The infeasible contact areas are marked with stripes in Figure 9. Thus, there is a given (short) distance where it is preferred that passing wheels of different shapes make their transition from wing rail to crossing nose or vice versa.

4.1. *Derivations*

In this section expressions will be derived for the contact point trajectories on crossing and wheel before these expressions are combined to derive expressions for the crossing-wheel interaction.

4.1.1. Contact point trajectories

First the linear functions that describe the lateral and vertical position of the contact point trajectories on wing rail and crossing are defined as a function of the longitudinal coordinate x using linear functions on the form $y = kx + m$ where k is the inclination of the curve and m the vertical off-set of the curve at $x = 0$. x equal to zero correspond to the Theoretical Crossing Point. The variable substitution $= \frac{t}{\alpha}$, where t is the nominal thickness of the crossing nose, is performed to find a parameterisation that is independent of the crossing angle α. The equations become

$$y_{\mathrm{wr}} = m_{\mathrm{wr},y} - \rho\alpha x = \left\{x = \frac{t}{\alpha}\right\} = m_{\mathrm{wr},y} - \rho t \quad (3)$$

$$z_{\mathrm{wr}} = K_{\mathrm{wr}}\alpha x = \left\{x = \frac{t}{\alpha}\right\} = K_{\mathrm{wr}} t \quad (4)$$

$$y_{\mathrm{cr}} = m_{\mathrm{cr},y} \quad (5)$$

$$z_{\mathrm{cr}} = K_{\mathrm{cr}}\alpha x + m_{\mathrm{cr},z} = \left\{x = \frac{t}{\alpha}\right\} = K_{\mathrm{cr}} t + m_{\mathrm{cr},z} \quad (6)$$

Here y_{wr} and y_{cr} are the lateral contact positions on wing rail and crossing nose respectively and z_{wr} and z_{cr} the corresponding vertical positions. For y_{wr} the constants for these investigations are determined using a least squares regression of the wing rail contact point trajectories of Figure 5 for the section where the contact points of wing rail and crossing nose overlap (from ~300 mm to ~750 mm). The same approach is used for the crossing nose, but here a constant value is deemed sufficient due to the small (2.5 mm) average change in lateral contact position in the overlap zone. The average contact position in the overlap zone according to the regression is therefore used. The determined values are presented in Table 1.

Variable	Value
$m_{\mathrm{wr},y}$	-33 [mm]
ρ	0.51 [-]
$m_{\mathrm{cr},y}$	27 [mm]

Table 1. Parameters for contact point locations determined using least squares linear regression

The lateral contact point trajectories are illustrated for the transition zone in Figure 10. Examples of the vertical contact point trajectories on the wing rail and crossing nose are shown in Figure 11.

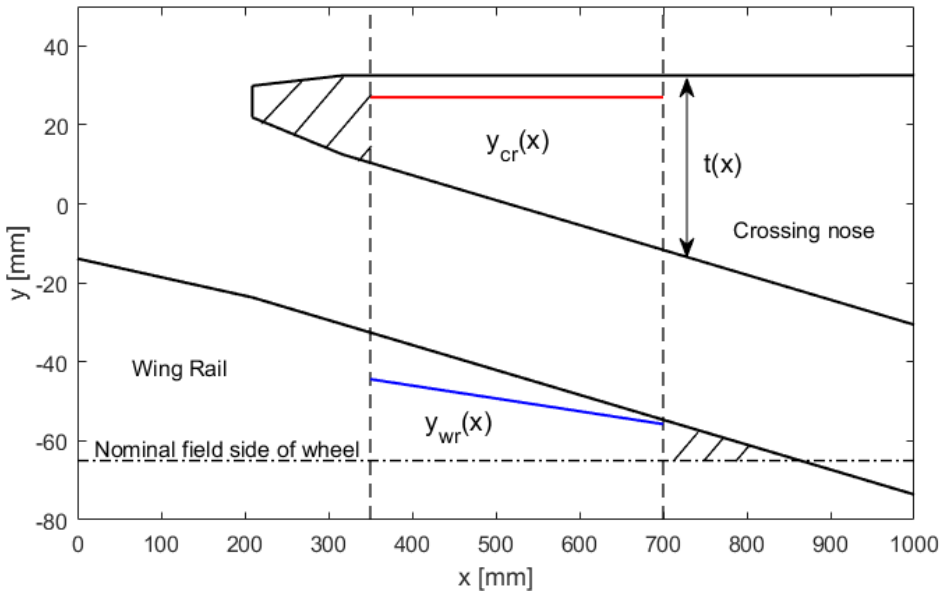

Figure 10. Prescribed lateral contact point trajectories in the transition zone using linear functions.

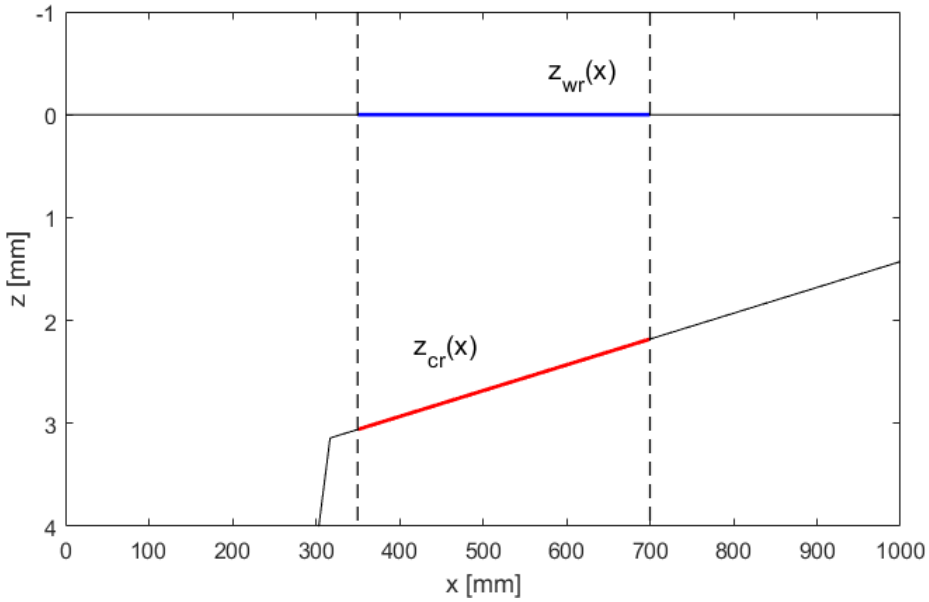

Figure 11. Schematic vertical-longitudinal cross-section illustrating vertical contact point trajectories in the transition zone of a crossing.

The constants that define the contact point trajectories in the vertical dimension ($K_{\mathrm{wr}}, K_{\mathrm{cr}}$ and $m_{\mathrm{cr},z}$) will be determined later through the adjustment of the crossing geometry to a given range of wheel profile cone angles. There is no $m_{\mathrm{wr},z}$ as this value is set to zero by default to lock the origin of the wing rail to $z = 0$ at $x = 0$.

4.1.2. Wheel profiles

The wheel profiles are modelled as conical and the wheel profile shape can then be described using the equivalent cone angle of Eq. (1) as

$$z_{\mathrm{wheel}} = \varphi y_{\mathrm{wheel}} \quad (7)$$

where φ is the equivalent cone angle of the wheel and y_{wheel} the lateral coordinate relative to the wheel's nominal rolling circle. The wheel is constrained laterally such that $y_{\mathrm{wheel}} = y$ at all times. Equation (7) together with the lateral positions for the contact points, (3) and (5), yield the vertical positions on the wheel at the lateral contact point locations.

$$z_{\mathrm{wheel,wr}} = \varphi(m_{\mathrm{wr,y}} - \rho t) \quad (8)$$

$$z_{\mathrm{wheel,cr}} = \varphi m_{\mathrm{cr,y}} \quad (9)$$

4.1.3. Wheel-crossing interaction

A cross-section view illustrating the wheel geometry and the vertical distances at the contact points is presented in Figure 12.

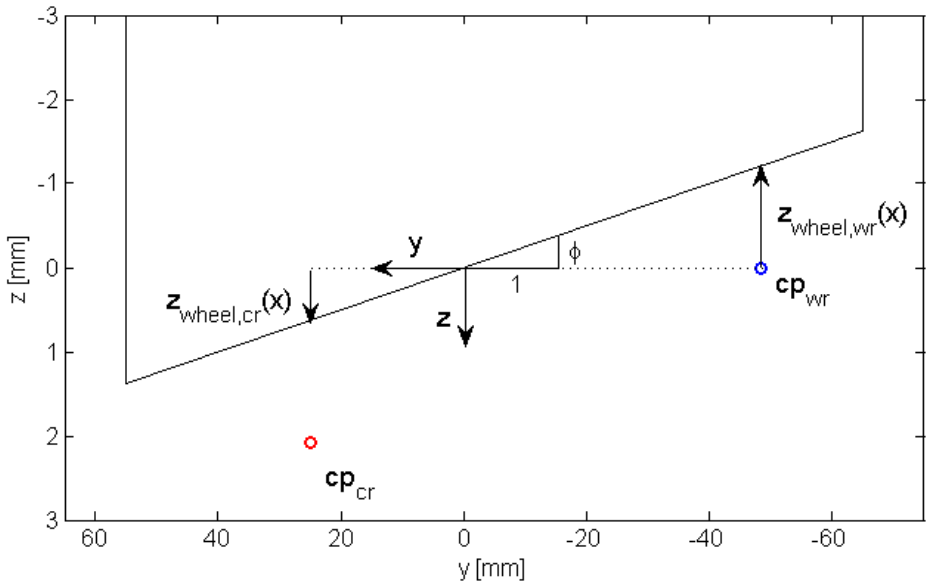

Figure 12. Cross-section of wheel profile and example contact point locations on wing rail and crossing nose.

The vertical wheel position p when the wheel is in contact with either wing rail or crossing nose can then be obtained by adding the vertical position of the contact point in question and subtracting the height of the wheel profile at the contact point relative to the wheel profile's origin. Using Eqs. (4),(6),(8) and (9) it is obtained that

$$p_{\mathrm{wr}} = z_{\mathrm{wr}} - z_{\mathrm{wheel,wr}} = K_{\mathrm{wr}}t - \varphi\left(m_{\mathrm{wr,y}} - \rho t\right) = K_{\mathrm{wr}}t + \varphi\left(\rho t - m_{\mathrm{wr,y}}\right) \quad (10)$$

$$p_{\mathrm{cr}} = z_{\mathrm{cr}} - z_{\mathrm{wheel,cr}} = K_{\mathrm{cr}}t + m_{\mathrm{cr,z}} - \varphi m_{\mathrm{cr,y}} \quad (11)$$

As the wheel position on the wing rail describes a downwards trend (towards increasing p) and the wheel position on the crossing describes an up-going trend (towards decreasing p), the transition point can be found at the intersection when $p_{wr} = p_{cr}$. Setting equations (10) and (11) equal yields

$$K_{\mathrm{wr}}t + \varphi\left(\rho t - m_{\mathrm{wr,y}}\right) = K_{\mathrm{cr}}t + m_{\mathrm{cr,z}} - \varphi m_{\mathrm{cr,y}} \quad (12)$$

Which yields that the crossing thickness at the transition point can be expressed as

$$t_{\mathrm{trans}} = \frac{m_{\mathrm{cr,z}} + \varphi(m_{\mathrm{wr,y}} - m_{\mathrm{cr,y}})}{\rho\varphi + K_{\mathrm{wr}} - K_{\mathrm{cr}}} \quad (13)$$

or as a function of the longitudinal position x (obtained via the variable substitution $t = \alpha x$)

$$x_{\mathrm{trans}} = \frac{m_{\mathrm{cr,z}} + \varphi(m_{\mathrm{wr,y}} - m_{\mathrm{cr,y}})}{\alpha(\rho\varphi + K_{\mathrm{wr}} - K_{\mathrm{cr}})} \quad (14)$$

The impact angle β can then be expressed as the difference in vertical wheel trajectory inclination of the wing rail and crossing nose at the transition point. First calculating the relevant derivatives

$$\frac{dp_{\mathrm{wr}}(x)}{dx} = \frac{d\left[K_{\mathrm{wr}}\alpha x + \varphi\left(\rho\alpha x - m_{\mathrm{wr,y}}\right)\right]}{dx} = \alpha(K_{\mathrm{wr}} + \rho\varphi)$$
$$\frac{dp_{\mathrm{cr}}(x)}{dx} = \frac{d[K_{\mathrm{cr}}\alpha x + m_{\mathrm{cr,z}} - \varphi m_{\mathrm{cr,y}})]}{dx} = \alpha K_{\mathrm{cr}} \quad (15)$$

and computing the inclination difference at a transition point yields

$$\beta = \frac{dp_{\mathrm{wr}}(x_{\mathrm{trans}})}{dx} - \frac{dp_{\mathrm{cr}}(x_{\mathrm{trans}})}{dx} = \alpha(K_{\mathrm{wr}} + \rho\varphi) - K_{\mathrm{cr}}\alpha = \alpha(\rho\varphi + K_{\mathrm{wr}} - K_{\mathrm{cr}}) \quad (16)$$

It can thus be observed that the impact angle is proportional to the inclination of the wing rail and crossing nose as well as the cone angle of the wheel. It can also be noted that there is no explicit x-dependence for β, but wheels with a larger cone angle will make an earlier transition and the impact angles will be larger for these wheel profiles according to this model (for $\rho > 0$). K_{wr} and K_{cr} can either be taken from an existing crossing design, or they can be determined from the range of wheel profile conicities

that are going to pass over the crossing. The latter procedure will be used in the following to determine the K_{wr} and K_{cr} required for a given range of wheel profile shapes to pass over the crossing in an orderly manner. These inclinations will correspond to the average impact angle that passing wheel profiles will experience as they roll over the crossing. Please note that K_{wr} and K_{cr} correspond to the inclinations of the average contact point trajectory on the wing rails and crossing nose. They are therefore not directly comparable to top-of-rail inclinations.

4.2. *Crossing geometry adjustment*

Assuming an extension of the transition zone as illustrated in Figure 10 and assuming a maximum and minimum cone angle wheel that should pass over the crossing, the vertical inclination of wing rail and crossing nose can be determined. By inserting t_{s}, which is the crossing nose thickness at the start of the transition zone, and equivalent wheel cone angle φ_{s}, which is the largest cone angle wheel that should pass over the crossing, into Eq. (12) it is obtained that.

$$K_{\mathrm{wr}}t_{\mathrm{s}} + \varphi_{\mathrm{s}}\left(\rho t_{\mathrm{s}} - m_{\mathrm{wr,y}}\right) = K_{\mathrm{cr}}t_{\mathrm{s}} + m_{\mathrm{cr,z}} - \varphi_{\mathrm{s}}m_{\mathrm{cr,y}} \qquad (17)$$

By inserting t_{e} (which is the crossing nose thickness at the end of the transition zone) and wheel cone angle φ_{e} (which is the smallest cone angle wheel that should pass over the crossing) into Eq. (12) it is obtained that.

$$K_{\mathrm{wr}}t_{\mathrm{e}} + \varphi_{\mathrm{e}}\left(\rho t_{\mathrm{e}} - m_{\mathrm{wr,y}}\right) = K_{\mathrm{cr}}t_{\mathrm{e}} + m_{\mathrm{cr,z}} - \varphi_{\mathrm{e}}m_{\mathrm{cr,y}} \qquad (18)$$

Through these equations dependencies have been created between the wheel profiles that should make their transitions at the start and end of the transition zone, and the wing rail and crossing nose inclinations and vertical positions. By subtracting (18) from (17), it is obtained that

$$\begin{aligned} &K_{\mathrm{wr}}(t_{\mathrm{s}} - t_{\mathrm{e}}) + \rho(\varphi_{\mathrm{s}}t_{\mathrm{s}} - \varphi_{\mathrm{e}}t_{\mathrm{e}}) + m_{\mathrm{wr,y}}(\varphi_{\mathrm{e}} - \varphi_{\mathrm{s}}) = \\ &K_{\mathrm{cr}}(t_{\mathrm{s}} - t_{\mathrm{e}}) + m_{\mathrm{cr,y}}(\varphi_{\mathrm{e}} - \varphi_{\mathrm{s}}) \end{aligned} \qquad (19)$$

By performing the variable substitutions

$$\varphi_{\mathrm{e}} = \varphi_{\mathrm{s}} - \delta \qquad (20)$$

$$t_{\mathrm{e}} = t_{\mathrm{s}} + T \qquad (21)$$

where δ is the wheel cone angle range ($\delta = \varphi_{\mathrm{s}} - \varphi_{\mathrm{e}}$) and T the crossing thickness change ($T = t_{\mathrm{e}} - t_{\mathrm{s}}$) in the transition zone, K_{cr} and K_{wr} can be extracted as

$$K_{\mathrm{cr}} - K_{\mathrm{wr}} = \rho\varphi_{\mathrm{s}} + \frac{\delta(m_{\mathrm{wr,y}} - m_{\mathrm{cr,y}} - \rho(t_{\mathrm{s}} + T))}{T} \qquad (22)$$

K_{cr} and K_{wr} are now solved for using the criterion that the average wheel trajectory slope should be the same for wheel trajectories on both wing rail and crossing nose. As the vertical wheel positions on wing rail and crossing nose are linear functions in φ, the criterion is formulated saying that the slope of the vertical wheel trajectory should be equal but opposite on the wing rail and crossing nose at the transition point of a wheel with average cone angle. This condition can be written as

$$\frac{dp_{\mathrm{wr}}(x_{\mathrm{trans},\varphi})}{dx} + \frac{dp_{\mathrm{cr}}(x_{\mathrm{trans},\bar{\varphi}})}{dx} = 0 \quad (23)$$

where the average wheel cone angle is defined as

$$\bar{\varphi} = \frac{\varphi_{\mathrm{s}} + \varphi_{\mathrm{e}}}{2} \quad (24)$$

Inserting Eq. (15) and (24) into (23) it is obtained that

$$\alpha(K_{\mathrm{wr}} + \rho\bar{\varphi}) + \alpha K_{\mathrm{cr}} = 0 \quad (25)$$

Which can be written as

$$\alpha\left(K_{\mathrm{wr}} + K_{\mathrm{cr}} + \rho\left(\varphi_{\mathrm{s}} - \frac{\delta}{2}\right)\right) = 0 \quad (26)$$

And yields

$$K_{\mathrm{wr}} = \rho\left(\frac{\delta}{2} - \varphi_{\mathrm{s}}\right) - K_{\mathrm{cr}} \quad (27)$$

(27) in (22) gives

$$2K_{\mathrm{cr}} - \rho\left(\frac{\delta}{2} - \varphi_{\mathrm{s}}\right) = \rho\varphi_{\mathrm{s}} + \frac{\delta(m_{\mathrm{wr,y}} - m_{\mathrm{cr,y}} - \rho(t_{\mathrm{s}} + T))}{T} \quad (28)$$

Which can be written as

$$K_{\mathrm{cr}} = \delta\left(\frac{m_{\mathrm{wr,y}} - m_{\mathrm{cr,y}} - \rho t_{\mathrm{s}}}{2T} - \frac{\rho}{4}\right) \quad (29)$$

It can be seen that the crossing nose inclination will have to be proportional to the wheel cone angle range δ and inversely proportional to the crossing nose thickness range in the transition zone, T. Given numerical values, the crossing geometry can now be determined for a given wheel profile range.

5. Model demonstration

In this section the properties of the derived model will be investigated from two perspectives; 1) Compared to the multi body simulations and 2) Through the derivation of the average impact angle for a given range of wheel profiles and the qualitative insights that can be drawn from this equation.

5.1. *Comparison to multi body simulations*

In order to compare the results of the quasi-static multi body simulations presented in Section 3 and the linear model, the linear model is adjusted to the same crossing geometry and wheel profile set. The range of wheel profile cone angles that should fit in the nominal transition zone is determined by first using Eq. (2) with the coordinates $x_{\mathrm{s}} = 350$ and $x_{\mathrm{e}} = 700$ mm to calculate the equivalent wheel cone angles at the start φ_{s} and stop φ_{e} of the transition zone, respectively. These coordinates correspond to crossing nose thicknesses of $t_{\mathrm{s}} = 22.1$ and $t_{\mathrm{e}} = 44.2$ mm (and thus $T = 22.1$ mm)

derived from a crossing angle $\alpha = 1/15.84$ which is the effective crossing angle of the reference geometry. The cone angle range itself is then calculated using Eq. (20) and becomes $\delta = \varphi_s - \varphi_e$=35.3 mrad. The values for constants $m_{wr,y}$, $m_{cr,y}$ and ρ are taken from **Error! Reference source not found.**. The constants K_{wr} and K_{cr} can then be calculated from (27) and (29) while the constant $m_{cr,z}$ can be calculated using for example Eq. (12).

Figure 13 (a) presents the correlation between the transition points calculated using (14) and the multi body simulations for all 400 wheel profiles. It can be observed that there is a strong agreement between the models as could be expected from the strong correlation between the equivalent cone angle and the transition point and the fact that the linear model was fitted to the wheel profile range that fit inside of the nominal transition zone in the MBS simulations. The correlation isn't perfect however. It is slightly banana shaped and the correlation is off for the (hollow) worn wheel profiles that make their transition outside of the transition zone beyond 700 mm. It can also be observed that this correlation is for a nominal crossing geometry. The crossing geometry will change in track due to wear and plastic deformation[9, 10].

Figure 13 (b) presents the impact angles as a function of transition point for all 400 wheel profiles for both models. The impact angles for the linear model are calculated according to Eq. (16). As can be observed the correlation is poor with respect to the impact angle of individual wheel profiles. As can be seen in Eq. (16), the linear model predicts a larger impact angle for wheel profiles with a larger equivalent cone angle and those wheel profiles make an earlier transition to the crossing nose. For the actual crossing geometry in the MBS simulations the impact angles are small for the early transition and then increase. The MBS simulations also demonstrate large individual impact angles for transitions outside of the nominal transition zone that are not captured by the linear model. Numerically calculating the average impact angle for all wheel profiles for both models it becomes $\bar{\beta}_{lin} = 7.7$ mrad for the linear model and $\bar{\beta}_{MBS} = 6.8$ for the multi body simulations. The linear model thus over predicts the average impact angle for this set of wheel profiles. It should be noted that the averages depend upon the distribution of cone angles in this specific wheel profile sample (which is not uniform) as the impact angles vary along the transition zone.

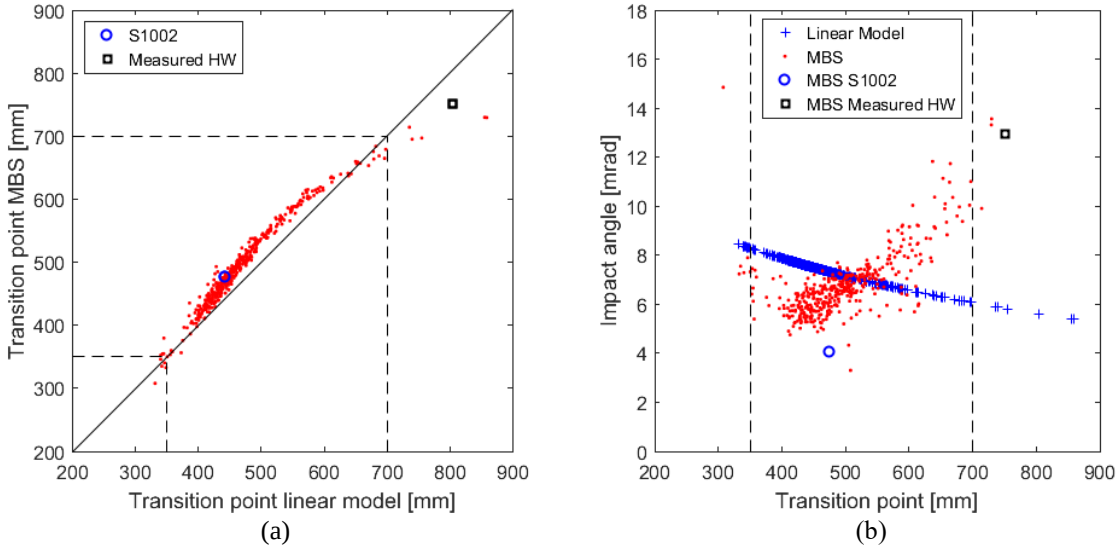

(a) (b)

Figure 13. (a) Correlation plot between wheel transition points for the linear model and multi body simulations. (b) Comparison of impact angles for analytical model and multi body simulations. Results for 400 wheel profiles

The differences between the MBS simulations and the linear model is further illustrated in Figure 14. It presents the vertical wheel trajectories in and around the transition zone for a nominal S1002 profile and a hollow worn profile in both the MBS and the linear model. Consistent with results in Figure 13 the agreement is good in terms of transition points, but there is little agreement between the shapes of the vertical wheel trajectories for individual wheel profiles that in turn determine the impact angles.

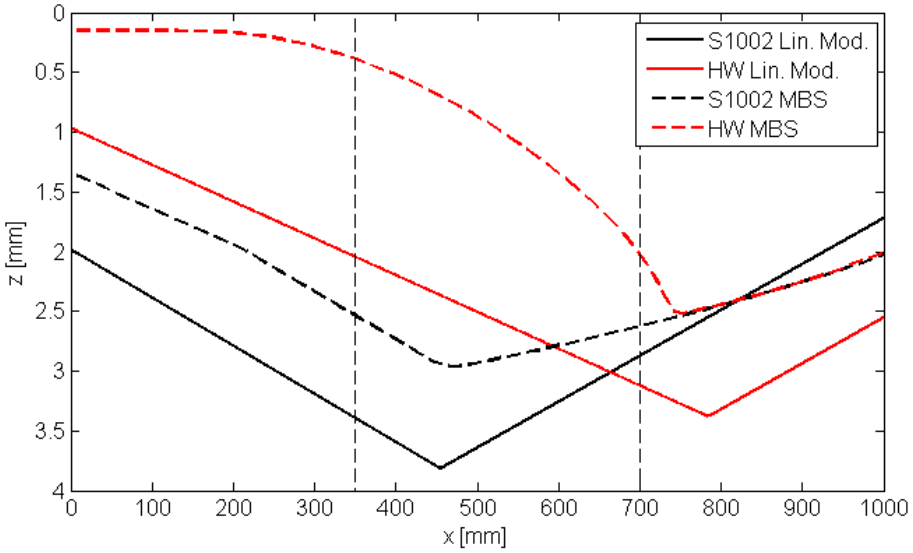

Figure 14. Comparison of vertical wheel trajectories for a nominal S1002 wheel profile and a hollow worn profile (HW) in the linear model and the multi body simulations

5.2. *Average impact angle*

The average impact angle $\bar{\beta}$ is obtained by inserting the average φ as $\bar{\varphi} = \varphi_s - \frac{\delta}{2}$ and Eq. (27) for K_{wr} into (16). This procedure gives the average impact angle as the impact angle is a linear function in φ. It is obtained that

$$\bar{\beta} = \alpha\left(\rho\left(\varphi_s - \frac{\delta}{2}\right) + \rho\left(\frac{\delta}{2} - \varphi_s\right) - K_{cr} - K_{cr}\right) = -2\alpha K_{cr} \qquad (30)$$

Inserting Eq. (29) further yields that

$$\bar{\beta} = \alpha\delta\left(\frac{\rho t_s + m_{cr,y} - m_{wr,y}}{T} + \frac{\rho}{2}\right) \qquad (31)$$

According to this model, it can be concluded that the average impact angle for wheels that pass over a fixed crossing is proportional to the crossing angle α, inversely proportional to the crossing nose thickness range T in the transition zone and proportional to the range of wheel profile equivalent cone angles δ that should be able to pass over the crossing with transitions in the nominal transition zone. With a smaller range of wheel profile shapes in traffic it would thus be possible to adjust crossing geometries accordingly and reduce impact angles and thus also reduce impact forces and associated degradation. Note that the crossing and wing rail inclinations K_{cr} & K_{wr} are implicit dependants in (31). When the variables change in this equation K_{cr} & K_{wr} change as well to accommodate a certain range of wheel profiles within the given transition zone. The constants of the contact point trajectories also have their influence, but the range of realistic values for these variables is limited. To see this two extreme examples are presented. First assume that the passing wheels have perfectly straight

contact point trajectories on the wing rail ($\rho = 0$, constant y-coordinate). Then (31) is reduced to

$$\bar{\beta} = \alpha\delta\left(\frac{m_{\mathrm{cr,y}} - m_{\mathrm{wr,y}}}{T}\right) \quad (32)$$

It can be observed that the impact angle can be reduced slightly if the distance between the contact bands is reduced (i.e. a smaller difference between $m_{\mathrm{cr,y}}$ and $m_{\mathrm{wr,y}}$). This could for example be achieved via a narrower flange way and profile optimization, but there is not much design margin to play with here given constraints on load bearing capacity and tolerances for flange passages. As a side note it can be mentioned that if the constants are chosen as in Eq. (1), $y_{\mathrm{cr}} = m_{\mathrm{cr}} = 25$ and $y_{\mathrm{wr}} = m_{\mathrm{wr}} = -55$, the product $\delta(m_{\mathrm{cr,y}} - m_{\mathrm{wr,y}})$ is equal to the range of height variation between flange root and field side for the wheel profile sample. In[4] this range was labelled Δ and by inserting it into (32) it is obtained that

$$\bar{\beta} = \frac{\Delta\alpha}{T} = \left\{\alpha = \frac{T}{L}\right\} = \frac{\Delta}{L} \quad (33)$$

which is identical to the expression derived in[4] using geometric reasoning. This equation now falls out as a special case of this more general modelling. Another extreme case is $\rho = 1$ which means that the contact point trajectory on the wing rail runs parallel with the gauge corner. Eq. (31) then becomes

$$\bar{\beta} = \alpha\delta\left(\frac{t_{\mathrm{s}} + m_{\mathrm{cr,y}} - m_{\mathrm{wr,y}}}{T} + \frac{1}{2}\right) \quad (34)$$

The resulting average impact angles will now be calculated and compared for equations (31),(32) and (34). The only difference between the equations is the trajectory for the lateral contact point on the wing rail. For all cases $m_{\mathrm{wr,y}}$ is adjusted such that it passes through the point $x = 700$ and $y = -55$. Summing up there is thus one case where the lateral contact point location has a constant lateral coordinate. Another where the contact point is parallel to the edge of the wing rail and one intermediate case. These cases are summarised in Table 5.1.

Equation	$m_{\mathrm{wr,y}}$	ρ	$\bar{\beta}$ [mrad]
(31)	-33	0.51	7.8
(32)	-55	N/A	8.3
(34)	-11	N/A	7.2

Table 5.1 Comparison of average impact angles

It can be observed that there is a slight difference in the estimated average impact angle between the equations. The explanation for this is that the smaller the average difference is in the distance between the lateral contact point locations on wing rail and crossing nose, the smaller K_{cr} and K_{wr} and the corresponding impact angle can be. This is because a given variation in equivalent cone angles gives a smaller variation in height difference between the field side and flange root side of the wheel profile if the lateral distance between the contact points is smaller. An extreme thought example to illustrate this point is to have the contact points of the wing rail and crossing nose coincide laterally. The impact angle can then be zero as all wheel profiles can be supported at a single point by both wing rail and crossing nose and the variation in wheel profile

shapes will not matter. For practical design purposes this means that one can strive to design crossing geometries that can minimize the span of height difference between wheels' contact points on wing rail and crossing nose.
Figure 15 illustrates the origins of the difference in average impact angle between equations (32) and (34). In this figure all wheel profiles are positioned on their contact point on the wing rail. It is shown that the span in height difference between contact points on the wing rail and crossing nose can be reduced for a set of wheel profiles if the lateral contact point location on the wing rail varies as in Eq. (34) compared to the uniform contact situation associated with Eq. (32). The contact point trajectories presented here are of course idealized, but they illustrate that the design of the wing rail and crossing nose rail profiles matter not only for the optimization of wheel rail contact, but also for the global design of the crossing.

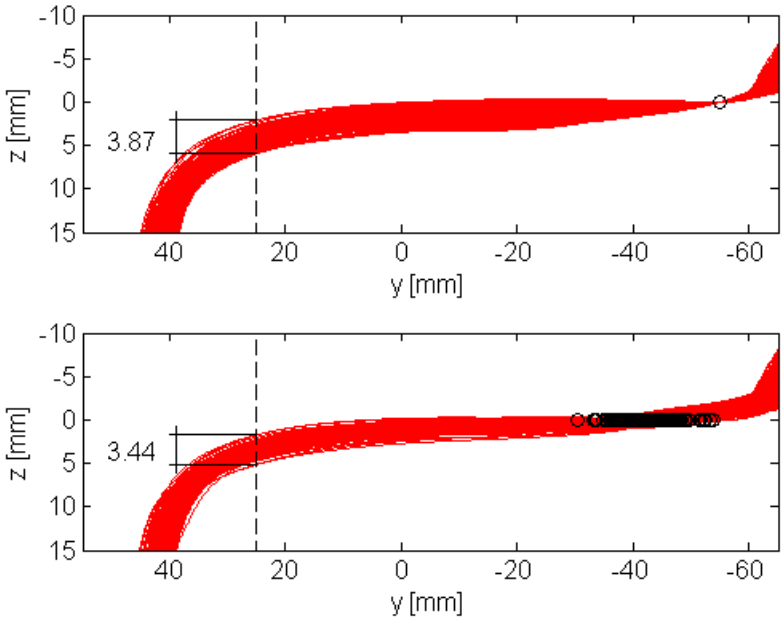

Figure 15. Span of height variation between nominal contact points on wing rail and crossing nose for wheel profiles associated with Equation (32) (Top) and Equation (34) (Bottom)

6. Conclusions

This paper has presented the derivation of a linear analytical model that describes the wheel-rail interaction kinematics in the transition zone of a crossing. Its properties have also been compared to quasi-static multi body simulation results for a set of 400 wheel profiles. The comparison has shown that the model shows good agreement in the estimation of transition points for individual wheel profiles and the average impact angle for this set of wheel profiles. The agreement is however poor in terms of capturing the impact angles and vertical wheel trajectories of individual wheel profiles as they pass over the crossing.
The model has allowed for the derivation of an expression that approximately determines the average impact angle (and corresponding inclinations of the contact point trajectories on wing rail and crossing nose in the traffic direction) that results if a certain range of wheel profile shapes should make an orderly transition at a crossing within a given transition zone. Good knowledge of the range of wheel profile shapes in traffic is therefore of importance if a crossing is to be optimized for a given traffic situation.

In addition the model imply the following for the optimization of railway crossings. A larger crossing angle increase the average impact angle which in turn increases impact forces and degradation for a given line speed. If crossing longevity is the only selection criterion it is thus better to use a larger radius turnout with a smaller crossing angle over a small radius turnout with a larger crossing angle. Further the model suggests that impact angles can be reduced if the crossing material is more damage resistant such that wheel transitions can be accepted further towards the tip of the crossing nose where it is thinner or where the overlap between wheel profiles and wing rail is small. Finally the model suggests that average impact angles can be reduced if lateral offset between the contact points on wing rail and crossing nose is smaller. Changes in this direction can for example be obtained via optimization of crossing nose and wing rail cross-sections and by keeping the flange way width as small as possible.

7. Acknowledgements

The work presented in this paper has been carried out within the project In2Rail which is a part of the European Union's Horizon 2020 research and innovation programme under Grant Agreement No. 635900. The work has been performed within the CHARMEC Centre of Excellence at Chalmers University of Technology.

8. References

1. Nicklisch D, Kassa E, Nielsen JCO, et al. Geometry and stiffness optimization for switches and crossings, and simulation of material degradation. *P I Mech Eng F-J Rai* 2010; 224: 279-292. DOI: Doi 10.1243/09544097jrrt348.
2. Wan C, Markine VL and Shevtsov IY. Improvement of vehicle-turnout interaction by optimising the shape of crossing nose. *Vehicle Syst Dyn* 2014; 52: 1517-1540. DOI: 10.1080/00423114.2014.944870.
3. Wan C, Markine V and Dollevoet R. Robust optimisation of railway crossing geometry. *Vehicle Syst Dyn* 2016; 54: 617-637. DOI: 10.1080/00423114.2016.1150495.
4. Palsson BA. Optimisation of railway crossing geometry considering a representative set of wheel profiles. *Vehicle Syst Dyn* 2015; 53: 274-301. DOI: 10.1080/00423114.2014.998242.
5. Simpack. Version 2017.4, www.simpack.com (2017).
6. Palsson BA and Nielsen JCO. Track gauge optimisation of railway switches using a genetic algorithm. *Vehicle Syst Dyn* 2012; 50: 365-387. DOI: Doi 10.1080/00423114.2012.665167.
7. Palsson BA and Nielsen JCO. Wheel-rail interaction and damage in switches and crossings. *Vehicle Syst Dyn* 2012; 50: 43-58. DOI: 10.1080/00423114.2011.560673.
8. Bezin Y, Grossoni I and Neves S. Impact of wheel shape on the vertical damage of cast crossing panels in turnouts. *24th Symposium of the International-Association-for-Vehicle-System-Dynamics (IAVSD)*. Graz, Austria 2015, p. 1163-1172.
9. Pletz M, Daves W and Ossberger H. A wheel passing a crossing nose: Dynamic analysis under high axle loads using finite element modelling. *P I Mech Eng F-J Rai* 2012; 226: 603-611. DOI: 10.1177/0954409712448038.
10. Pletz M, Ossberger U, Ossberger H, et al. Dynamic finite element model-impact force and contact pressure for measured geometries of fixed crossings. *24th Symposium of the International-Association-for-Vehicle-System-Dynamics (IAVSD)*. Graz, Austria 2015, p. 1337-1346.